Eur. Phys. J. Spec. Top.
https://doi.org/10.1140/epjs/s11734-024-01398-7

THE EUROPEAN PHYSICAL JOURNAL SPECIAL TOPICS

Regular Article

Optimized battery electrodes with primer layers by simultaneous two-layer slot-die coating

Alexander Hoffmann[1,a], Julian Klemens[1], Sebastian Raupp[2], Christoph Hanske[2], Nils Lawrenz[2], Michael Machate[2], Philip Scharfer[1], and Wilhelm Schabel[1]

[1] Thin Film Technology, Karlsruhe Institute of Technology, 76131 Karlsruhe, Germany
[2] BASF SE, Carl-Bosch-Strasse 38, 67056 Ludwigshafen am Rhein, Germany

Received 30 July 2024 / Accepted 5 November 2024

Abstract Multi-layer coating is a promising method for optimizing the properties of battery electrodes. This study examines the simultaneous coating of anodes with a primer layer without the necessity of a second coating and drying step, as it is the case for sequential coating processes. The primer layer is used to concentrate the binder in proximity to the substrate, thereby enhancing the adhesion strength of the electrode. Two systems comprising anode and primer, differing in rheological properties, are selected for coating investigation. It is demonstrated that the viscosity ratio of the multi-layer coating has a pronounced effect on coating suitability. In a two-layer system, the viscosity ratio also changes with shear rate due to the possibly different shear thinning properties. This results in the observation that combinations with strong viscosity ratios might only be stable in specific coating speed ranges. In contrast, combinations with moderate viscosity ratios exhibit a reduction in stable process windows as the viscosity ratio between the top and bottom layer increases. A mechanical characterization of the adhesion strength of dried and calendered electrodes demonstrated a notable enhancement in adhesion strength when a primer was utilized. In addition, capacity retention tests revealed that the electrochemical properties were not adversely affected by the primer.

1 Introduction

In recent years, battery technology has undergone significant advancements. The development of new material systems has been accompanied by a reduction in production costs, with a 75% decrease observed over the past 10 years in the field of lithium-ion batteries (LIB) in general [1]. This has enabled the integration into a range of applications beyond consumer electronics, including high-energy and high-performance sectors in large-scale stationary energy storage and electric mobility. The characteristics of well-performing battery electrodes are energy density (volumetric and gravimetric), electrochemical properties (cycle stability, C-Rate capability), mechanical properties (adhesion strength of the electrode to the metal substrate) as well as process-related properties, for example the suitability of a material system for a high-speed coating and drying process.

The properties of a battery electrode can be defined or influenced during the coating and drying step. One aspect of the drying process is the migration of the binder in the electrode. During drying, a capillary transport of the liquid solvent toward the electrode surface occurs, resulting in the accumulation of binder at the wet coating surface [2–4]. An elevated local concentration of binder has a detrimental effect on the performance of the electrode, as the ionic and electric resistance in the pores increases [5–7]. A reduction in the concentration of binders can, in principle, reduce the ionic resistance and lead to an increase in performance. However, this may result in a reduction in adhesion between the substrate and the electrode. A more effective approach is to use a multi-layer system in which the electrode properties are graded along the height axis. A study conducted by Kumberg et al. on aqueous electrodes with a binder system of Carboxy–Methyl–Cellulose (CMC) and Styrene-Butadiene Rubber (SBR) demonstrated that by selecting an appropriate distribution of binder and active materials in a simultaneous multi-layer system, it is possible to accelerate drying rates without compromising the quality

[a] e-mail: alexander.hoffmann@kit.edu (corresponding author)

Published online: 26 November 2024

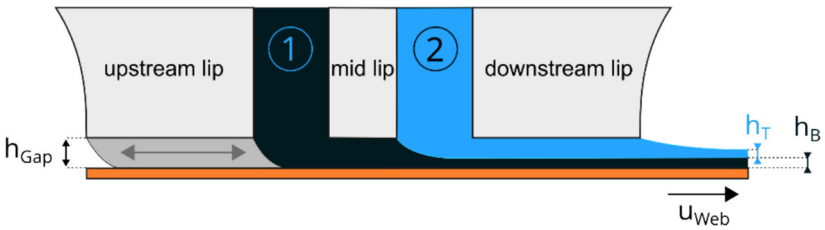

Fig. 1 Schematic side view of a two-layer slot die operating at stable conditions

or performance of the electrodes [8]. Diehm et al. successfully applied this concept with similar results to slot-die coating, maintaining the total binder content constant while shifting the binder to the lower layer in varying intensities [9]. Another study by Diehm et al. used a sequential coating approach to produce an electrode comprising an undercoated primer layer to enhance adhesion [10]. This method requires two sequential coating and drying stages, increasing financial costs for manufacturers by necessitating investment in an additional production line. In both cases, the binder content in the electrodes can be reduced without compromising electrode quality or performance.

In this study, the potential benefits of simultaneous coating of an anode with a primer layer are investigated. This approach combines the advantageous electrode properties using the primer layer, lowered binder content in the anode and the process simplification resulting from the 1-step coating solution.

The stability of the coating applied by a two-layer slot die is highly dependent on the material properties, such as the ratios of the viscosities and the volume flows of the individual layers and the difference in surface tension. Assuming an equal slot outlet width of the top and bottom layer, the volume flow ratio translates into the wet-film height ratio. In Fig. 1, a schematic side view of a two-layer slot die, operating at stable conditions, is presented with an indication of the gap height (h_{Gap}), top and bottom wet-film height (h_T, h_b), and web speed (u_{Web}).

To ensure the quality of the coating, it is necessary to adjust the process parameters in such a way that the menisci are stabilized in the positions shown in Fig. 1. This includes the menisci below the upstream lip (the interface between the bottom layer and the environment), below the middle lip (the interface between the two fluids), and at the downstream lip (the interface between the top layer and the environment). For unstable upstream menisci, e.g., due to insufficient volume flows of the bottom layer, which also corresponds to insufficient wet-film heights, air can be entrained in the fluid bridge between the slot die and the substrate (coating bead). This, or excessive differences in fluid properties, can also cause a shift in the fluid–fluid interface, which can lead to intermixing phenomena. The upper process boundary on the upstream side is defined by the swelling limit, which represents the point at which the fluid flows out of the upstream gap against the coating direction. In this case, on the downstream side, wetting of the die-side walls can occur, if the wet-film height exceeds the gap height. In addition, an unwanted expansion of the coating may occur, resulting in an overall deviation of the wet-film height.

The range of wet-film heights for a given set of process parameters, in which a defect-free coating is obtained, is referred to as the coating window. A universal and transferable unit of measurement is the dimensionless gap height G^*. This is defined as the ratio of the gap height to the wet-film height.

$$G^* = \frac{h_{\mathrm{Gap}}}{(h_B + h_T)} \tag{1}$$

From the perspective of coating science, the application of simultaneous primer coatings presents a series of scientific questions. Since dried primer layers are very thin (0.5–2 µm) compared to the electrode layers (typically $>$ 70 µm) and conventional primer slurries exhibit a solid content in the range of 1–5 wt% in comparison to 35–50 wt% of an anode slurry, the initial ratio of wet-film heights between the top and bottom layers is large. In the present study, for example, the wet-film thicknesses were in the range of 50 µm for the primers and 150 µm for the anodes. The combination of these factors results in viscosity and layer thickness ratios that may differ significantly from the optimum state of similar viscosity and layer thickness for each layer. Apart from flow-specific properties, surface tension differences may arise due to the formulations used.

In contrast to Newtonian fluids, for which the stability of a multi-layer coating is well described in the literature [11] and can be calculated using analytical models [12], the rheological behavior of shear-thinning fluids used here is also dependent on the shear rate and the associated coating speed. To investigate the influences on the coating stability, a suitable primer slurry formulation with low solid content and anode slurry formulation with high solid content are developed. To assess the impact of the coating speed, two coating systems are selected for investigation. These systems exhibit similar viscosity profiles for the individual top and bottom layer formulations at either lower shear rates (System-1) or higher shear rates (System-2). The operating window for stable coatings are experimentally investigated in relation to coating speed for both systems, with the objective of evaluating the suitability of the formulations for the simultaneous two-layer coating process. In view of the high-viscosity ratio that results for System-2, the introduction of a lip offset is also presented as a method of influencing the pressure

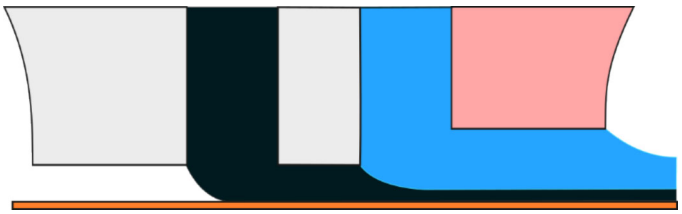

Fig. 2 Schematic representation of a lip offset in the downstream region

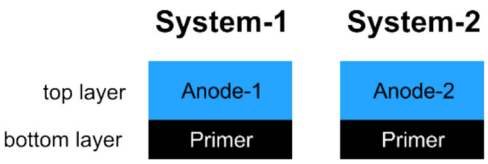

Fig. 3 Schematic illustration of the layer configuration in the material Systems-1 and -2

distribution in the coating bead. This involves shifting the downstream lip to a position that creates a greater gap than the upstream and middle lips. In the present study, the upstream and mid-gap height were established uniformly. The schematic view of a slot die with lip offset is illustrated in Fig. 2.

The upstream meniscus can be stabilized by positioning the upstream and middle lip in closer proximity to the substrate. This method is particularly suited to multi-layer coatings, such as those employed in the current study, where the top layer exhibits a significantly higher wet-film thickness than the bottom layer. Furthermore, the lip offset can result in a delay in the onset of mid-gap invasion. If mid-gap invasion occurs, the interface between the fluids in the coating bead can shift below the middle lip, pin on the upstream side of the middle lip or begin to oscillate, depending on the material properties and process parameters [13]. The pressure reduction in the upper layer as a result of the lip offset can delay the occurrence of turnaround flow or vortices, which can cause intermixing of the layers [13, 14].

System-1 is further used to fabricate electrodes on a pilot line and characterize them mechanically and electrochemically to measure the influence of the primer on battery cell level.

2 Materials and methods

2.1 Layer configuration and slurry preparation

In this study, two distinct multi-layer systems were investigated. The multilayer systems are based on a combination of the same primer slurry (primer) and different anode slurry (Anode-1, Anode-2), as illustrated in Fig. 3.

While the same primer slurry was used in both systems, the anode slurries differed in their composition. Anode-1 is derived from the formulation from the study conducted by Diehm et al. [9]. Anode-2 exhibits reduced CMC and SBR binder content and higher proportion of active material compared to Anode-1. It can be anticipated that the specific modification of the CMC proportion will have a significant influence on the viscosity of the slurry. An overview of the components of the individual slurries is presented in Table 1.

The slurries were prepared using a dissolver mixer (DISPERMAT CN 10, VMA-GETZMANN GmbH). Carbon Black was dispersed in a CMC-water solution with a lab stirrer. The active material content was incrementally augmented, and the subsequent dispersion phase was maintained under vacuum for a period of 45 min. Lastly, the SBR binders were added into the mixture at low mixing speed over a period of 10 min. To generate flow profiles with an altered viscosity, a lower CMC concentration was employed for Anode-2. The production of the primer formulations was conducted in accordance with the same methodology, except for the incorporation of the active material.

In the top layer slurries (Anode-1 and Anode-2), 0.5 wt% UV marker was added (Disodium 4,4′-*Bis*(2-sulfonatostyryl)biphenyl, DSBB, Tokyo Chemical Industry Co. Ltd.) to improve defect visibility in the coating experiments.

2.2 Rheology

The viscosity of the slurries was measured in dependence of the shear rate using a plate-plate-rheometer MCR-101 by Anton Paar with a 25 mm flat measuring head. Shear rate sweeps are performed from 0.01 to 1000 s^{-1}. In Fig. 4, the rheology profiles of System-1 and System-2 are shown.

Table 1 Formulations of the slurries used in the two-layer coatings

Slurry (system)	Material	Concentration/	
		wt% (wet)	wt% (dry)
Primer	Dispex Ultra PX 4585	0.04	1.96
	Carbon Black (C-NERGY Super C65)	0.83	40.69
	Thickener	0.54	26.47
	CMC (Texturecell 40,000 PA)	0.21	10.29
	SBR (Licity 2680)	0.42	20.59
	Water	97.96	
Anode-1	Graphite (SMG A, Hitachi)	35.33	95.38
	Carbon Black (C-NERGY Super C65)	0.53	1.43
	CMC (Walocell CRT 20000 PA 07)	0.71	1.92
	SBR (Licity 2680, BASF)	0.47	1.27
	Water	62.96	
Anode-2	Graphite (SMG A, Hitachi)	37.80	97.93
	Carbon Black (C-NERGY Super C65)	0.40	1.04
	CMC (Texturecell 40,000 PA)	0.20	0.52
	SBR (Licity 2680, BASF)	0.20	0.52
	Water	61.4	

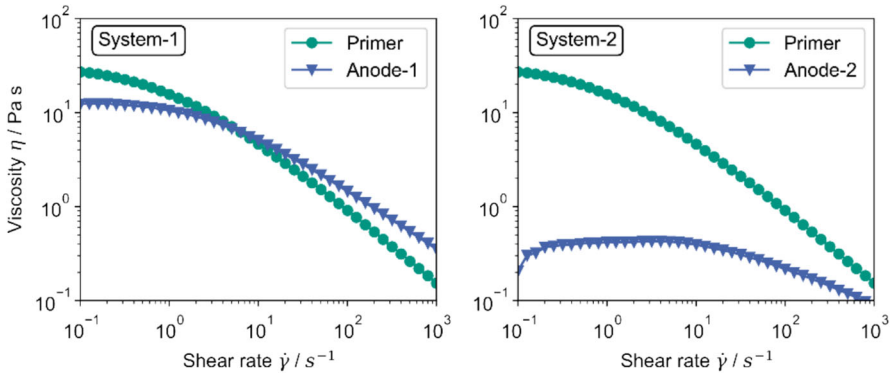

Fig. 4 Viscosity in dependence of the shear rate for primer and anode combinations, System-1 (left) and System-2 (right)

For System-1, the slurries were chosen to generate viscosity profiles that are as similar as possible with an overlap in lower shear rate regions. Both profiles intersect at approx. 1.5 s^{-1} (9 Pa s). The primer slurry shows stronger shear-thinning behavior (higher slope), leading to a spreading of the viscosity profiles with increasing shear rates. In System-2, the magnitude of the viscosity of Anode-2 is significantly lower. This was anticipated based on the reduction in the CMC proportion. Here, the two profiles gradually approach each other for increasing shear rates, but do not intersect in the measured range.

2.3 Characterization of coating stability

The coating experiments were conducted at the Development Coater (TSE) at the Thin Film Technology Laboratories. The basis of this system is a rotating steel roller, covering a speed range from 1 to 650 m min^{-1}. In the 8 o'clock position, a multi-layer slot die is mounted, which is fed by a high-precision dosing system (Nemesys, Cetoni GmbH). The coating is removed on the opposite side of the roller to allow an isolated view of the coating. The coating gap is adjusted by means of shim foils. The coating is observed by two cameras, one under the slot die on the upstream side to detect the swelling limit, the second is directed at the coating after the slot die outlet. To increase visibility of defects in the coating, a UV lamp is added to the setup, which illuminates the top layer of the coatings. Figure 5 shows a schematic illustration (left) and a photo (right) of the experimental setup.

A self-constructed two-layer slot die with a side-plate design was used. The upstream and downstream lip length was 1 mm, 0.8 mm in case of the middle lip. The die outlet was 60 mm wide.

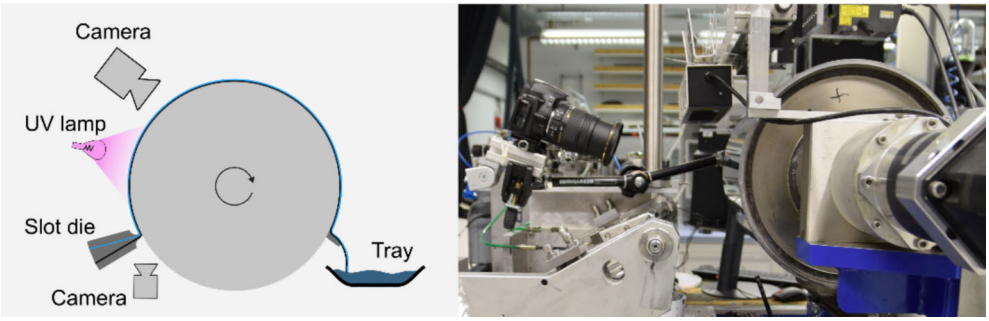

Fig. 5 Schematic illustration (left) and a photo (right) of the coating setup, including the slot die, camera 1 (upstream gap), camera 2 (die outlet and coating surface), UV lamp, measurement equipment and the blade with a tray for slurry collection

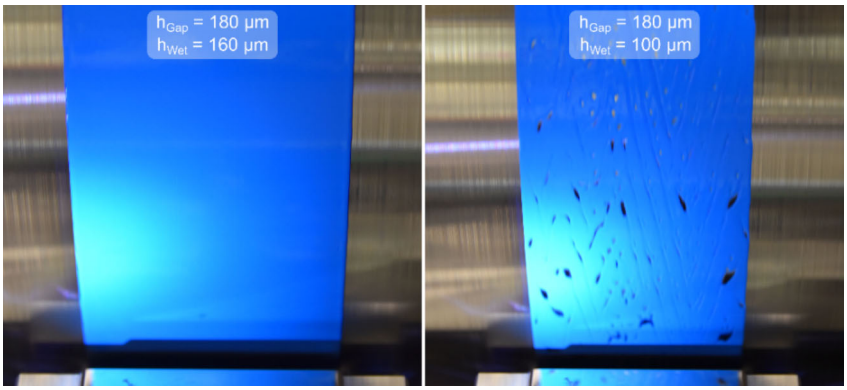

Fig. 6 Exemplary illustration of improved defect visibility by adding a UV marker in the top layer, showing a stable coating (left) and an unstable coating (right). With the UV marker, the top layer appears in blue color under a UV light, while the bottom layer remains black

To record the coating window, the rotation speed of the roller was set to the desired coating speed and the volume flow ratio between top and bottom layers (h_T/h_B) was kept constant at a value of three. The investigation was started at an unstable point in the air-entrainment regime, which represents the unstable lower area of process parameters. The volume flow was raised until the coating stabilizes. At this point, the lower limit was recorded. Volume flow was then raised continuously until swelling was detected or if the wet-film height exceeded the gap height to avoid wetting of die-lip shoulders or increased widening of the coatings. With the fluid coloring used, defect visibility is improved significantly, as presented in Fig. 6. This figure compares a stable coating on the left with an unstable coating on the right.

2.4 Pilot line

For electrode production, the pilot coater KTF-S by Mathis AG (2015) at BASF was used. The coating station was equipped with a two-layer slot die (RapidEdge Technology GmbH) with 220 mm coating width, adjusted by shim foils. To ensure complete coverage of the anode over the coating width, the coating width of the lower layer was reduced by 10 mm. In all experiments, the coating speed was set to 1 m min^{-1}. The pilot line has three dryer zones, in which the fan speed and the air temperature can be adjusted. The drying rate was calculated considering the heat transfer coefficient and the film temperature. The drying conditions for each zone are presented in Table 2.

Table 2 Drying conditions for two-layer coatings on the pilot line

System	Temperature/°C			Heat transfer coefficient/W m^{-2} K^{-1}		
	Zone 1	Zone 2	Zone 3	Zone 1	Zone 2	Zone 3
1	92	65	75	50	35	35
2	90	80	80	35	35	35

Table 3 C-rates at specific cycles during capacity retention tests

Cycles	C-Rate
Cycle 1 and 2	0.1 C
Cycle 25–27	0.2 C
Cycle 7, 8	0.33 C
Remaining cycles	0.5 C

2.5 Adhesion strength

Prior to the adhesion strength measurements, the electrodes were calendered using a GKL 300 L (Saueressig) at BASF with a target density of 1.5 g cm^{-3} at a process speed of 0.5 m min^{-1}, resulting in a line force of 120 N mm^{-1}. The adhesion strength was measured by conducting a 90° peel test with a TMTC-FR2.5TN.D09 (ZwickRoell GmbH & Co KG) machine. The electrodes were affixed with a strip of adhesive tape and subjected to a standardized weight force to ensure comparability of the results. The tape is then engaged in the clamping mechanism of the tensile testing machine. When starting the experiment, the machine head proceeds upwards with a constant velocity while maintaining a 90° angle. The electrode, which is attached to the tape, is pulled off the substrate, the force response is continuously recorded and subsequently averaged arithmetically. The experiment is conducted at least twice for each electrode.

2.6 Electrochemical characterization

To assess the electrochemical performance, capacity retention tests were conducted. These tests involve measuring the discharge capacity over a specified number of cycles on a Maccor Series 4000 Battery Tester (Maccor Inc., USA). For each two-layer configuration, an additional cell with an identical anode without primer coating was measured to illustrate the impact of the primer layer. The cathode electrode was composed of NCM831205 (94%) type active material, conductive carbon (C65, Imerys), graphite (SFG6L, Timcal), and a PVDF binder (Solef5130, Solvay) with an average areal capacity of ca. 2 mAh cm^{-2}. The electrode was compressed to 3.2 g cm^{-3} density with a laboratory calender (Sumet Technologies GmbH & Co. KG). Electrodes of 50 mm × 50 mm size were punched from the electrode and assembled to single-layer pouch cells together with the anodes and a Celgard 2500 separator (Celgard). 1 ml of electrolyte was filled into the cells. The electrolyte composed of 1 M $LiPF_6$ in EC:DEC 3:7 (wt) with 2 wt% VC as additive. The cells were formed at 25 °C with a degassing step after charging them to 4.2 V. Long-term cycling tests were carried out at 45 °C with ASR measurements of the cells after every 100 cycles at 25 °C. The cycle numbers with corresponding C-rate settings are presented in Table 3.

3 Results and discussion

3.1 Coating investigations for System-1

During the investigations of coating stability, the gap height and the individual wet-film heights in the multi-layer coating were kept constant according to Table 4. The ratio of the wet-film heights and volume flows of the individual layers was set to.

$$\frac{h_T}{h_B} = 3 \tag{2}$$

First, System-1 was investigated. In Fig. 7, a scatter plot of multiple points of operation is presented. Stable points are illustrated as green circles, unstable points in the bead-breakup regime (air entrainment) as red crosses,

Table 4 Coating parameters for stability investigations

Parameter	Value
Gap height h_{Gap}	210 µm
Top layer thickness h_T	150 µm
Bottom layer thickness h_B	50 µm
Coating width	60 mm

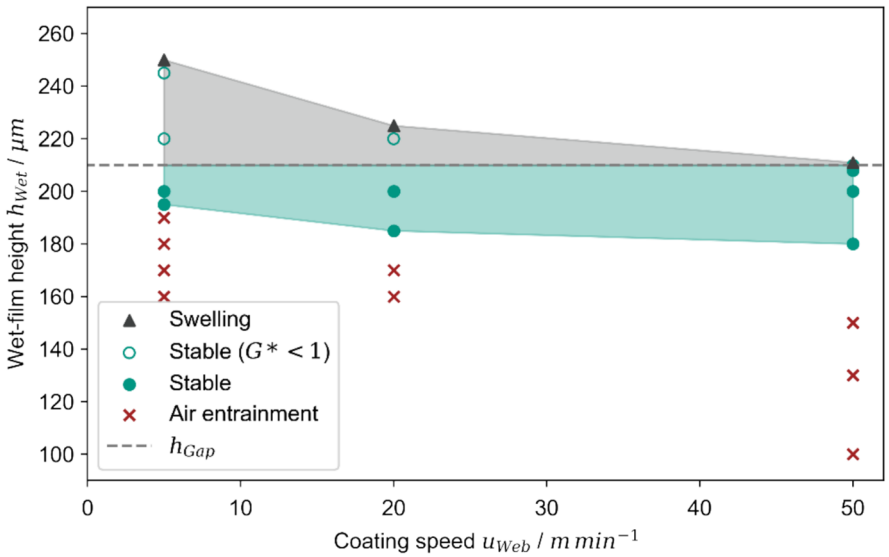

Fig. 7 Operation points for System-1 at different coating speeds producing unstable coatings with insufficient volume flows (red crosses), stable coatings (green circles), and unstable coatings with excessive volume flows (black triangles). The gap height is indicated as a grey dashed line, stable coatings exceeding the gap height as green, unfilled circles

and unstable points in the swelling regime as black triangles. Points recorded below $G^* = 1$ (wet-film height exceeds the gap height) without swelling are indicated as non-filled green circles. The stable coating window is characterized by green shading and straight-line connection of the speed-specific points, the area above $G^* = 1$ without an occurrence of swelling by a grey shading.

The data indicate that System-1 is well-suited for simultaneous multi-layer coating within the speed range under consideration. At the lowest speed of 5 m min^{-1}, a stable coating between 190 and 245 µm wet-film height was observed, which corresponds to a coating window with a width of 55 µm. As the speed is increased to 20 m min^{-1}, the coating window shifts downwards and becomes narrower, with a width of 35 µm. This trend continues for 50 m min^{-1}, with a width of 28 µm. If a constraint is applied to wet-film heights below the gap height ($G^* = 1$), a coating window of 15, 25, and 28 µm is obtained for 5, 20, and 50 m min^{-1}, respectively. The observed coating windows are sufficiently large to accommodate System-1 in a production process.

The stability range shows that the viscosity and wet-film height ratios have an influence on the width and position of the coating window. The study by Diehm et al., in which two-layer configurations with identical viscosity in both layers were investigated, is suitable for comparison with the data shown [9]. In their case, the process limits showed no clear influence of the process speed, but instead exhibited a constant coating window in the range of $0.95 < G^* < 1.4$, which corresponds to a width of approx. 45 µm for coating speeds between 5 and 20 m min^{-1}. In comparison to their findings, in this study, higher volume flows are necessary to stabilize the coating bead throughout the entire coating speed range. Regarding the upper limit, the onset of swelling in the study of Diehm et al. is found at $G^* = 0.95$. In the present study, higher wet-film heights were measured at low speeds ($G^* = 0.86$) and similar ranges at medium speeds ($G^* = 0.93$). Under the assumption that the constant trend in the study by Diehm et al. continues up to 50 m min^{-1}, lower values for the upper limits ($G^* = 1.01$) are found at high speeds.

This behavior is partly due to the wet-film height ratio. Since only the bottom layer is present under the middle lip, this is decisive for the stability of the upstream meniscus, as it must bridge the area between the die lip and the substrate. In this study, a wet-film height ratio of top to bottom of 3 is fixed, so that the total height of the coating results in higher values when the critical minimum thickness of the bottom layer is reached to stabilize the coating bead.

In addition, the coating window is influenced by the viscosity ratio, which is effective in the area of two-layer presence below the downstream lip. As previously shown in Fig. 4, the viscosity curve of the two layers changes differently with the shear rate. At higher coating speeds, the ratio between the viscosity of the top and bottom layers increases due to the higher shear rate, resulting in a change in the pressure drop created by the channel flow below the downstream lip, and therefore influencing the magnitude of volume flows necessary for a stable coating bead. The trend toward lower and narrower coating windows for increasing top-to-bottom viscosity ratios is also confirmed in numerical investigations for shear-thinning fluids [15] and can be approximated by comparing analytical calculations for Newtonian systems with different material combinations as suggested by Ji et al. [12].

Compared to single-layer electrodes, the coating window for multi-layer electrodes is significantly smaller. In the range of 5–50 m min^{-1}, high-viscosity battery slurries mainly show the air-entrainment defect, which occurs at a wet-film height corresponding to approximately half the gap distance [16]. If a simultaneous multi-layer coating process is chosen, the reduced coating window must be considered for positioning the slot die in the production process. In addition, the rheological behavior of the battery slurries significantly influences the stability range,

which can lead to a speed dependency with different slopes of the rheology profiles, as shown here. When scaling up production systems or changing the process speed, these correlations must also be considered to avoid instability.

3.2 Coating investigations for system-2

In System-2, the battery slurries show a different rheological behavior as shown in Fig. 4. At low shear rates (e.g., 1 s^{-1}), the viscosity ratio between the top and bottom layer is 39, while at higher shear rates, the profiles approach each other, up to a top-to-bottom viscosity ratio of 1.73 at 1000 s^{-1}. The effect of speed dependence is expected to be stronger than in System-1, so the range is resolved higher and stability tests are performed at 5, 10, 20, 30, 40, and 50 m min^{-1}. The coating window data are shown in Fig. 8. Stable points are illustrated as green circles, unstable points in the bead-breakup regime (air entrainment) as red crosses, and unstable points in the swelling regime as black triangles. Points recorded below $G^* = 1$ (wet-film height exceeds the gap height) without swelling are indicated as non-filled green circles. The stable coating window is characterized by green shading and straight-line connection of the speed-specific points, the area above $G^* = 1$ without an occurrence of swelling by a grey shading.

Stable coatings were only observed for 40 and 50 m min^{-1} in the area under investigation. For coating speeds of 5, 10, 20, and 30 m min^{-1}, it was not possible to produce a defect-free coating, as the streak defects caused by air entrainment went directly into the swelling limit without forming a stable area. The coating window at 40 m min^{-1} is between 198 and 213 µm (15 µm wide) and between 178 and 225 µm (47 µm wide) at 50 m min^{-1}. If one again assumes the limitation by the maximum at $G^* = 1$, the coating window for 40 m min^{-1} remains unchanged, while that at 50 m min^{-1} decreases to a width of 32 µm. From an industrial perspective, the coating window for 50 m min^{-1} would be large enough to use System-2 for the simultaneous coating process.

This data set confirmed the anticipated impact of coating speed on coating stability. In comparison to System-1, the greatest stable range is observed at high speeds (or shear rates), which aligns with the trends observed in the viscosity profiles. The quality of the coating can be more effectively depicted through images of the coating, as demonstrated in Fig. 9. For an improved visibility, the contrast in the excerpts shown for each coating was increased.

The bright stripes show the usual defect pattern of an unstable lower layer in the bead-breakup regime. This example illustrates that, depending on the viscosity ratio, a change in process speed can result in not only a shift or change of the coating window, but also in the inability to produce coatings at a target wet-film height with material systems like System-2 at all. Since the target film thickness can only be achieved within a certain range of speeds, any deviation from this range would require additional manipulations in the pressure conditions within the coating bead.

As a potential optimization strategy, a lip offset was investigated. The dimensioning of the lip offset is contingent upon the wet-film thickness of the upper layer. In this study, a lip offset of 130 µm was chosen, yielding a coating gap of 90 µm in both the upstream and mid regions, whereas the downstream coating gap was adjusted to 220 µm. This configuration was realized through the strategic placement of shim foils with precise thicknesses during assembly, thereby facilitating the displacement of the die blocks. The selection of lip offset dimensions was limited by the available shim thicknesses. The objective was to stabilize the operating point at coating speeds of

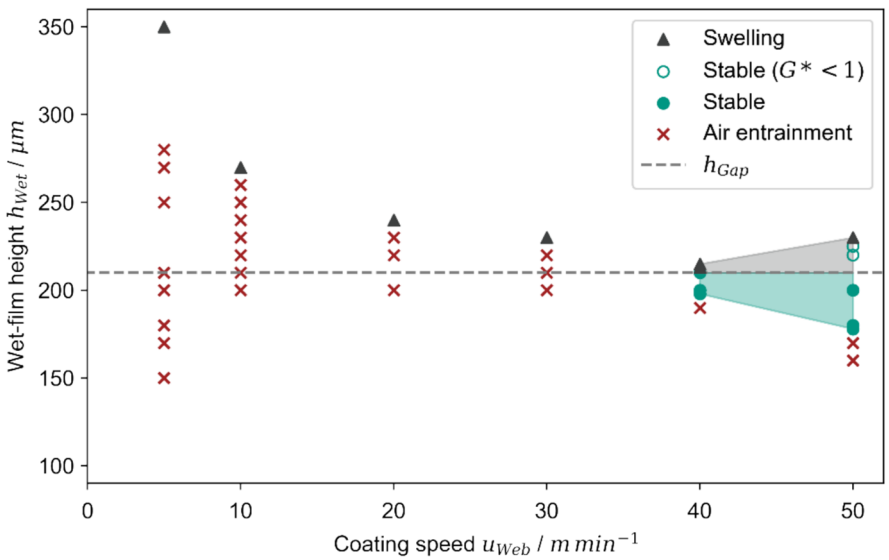

Fig. 8 Operation points for System-1 at different coating speeds producing unstable coatings with insufficient volume flows (red crosses), stable coatings (green circles), and unstable coatings with excessive volume flows (black triangles). The gap height is indicated as a grey dashed line, stable coatings exceeding the gap height as green, unfilled circles

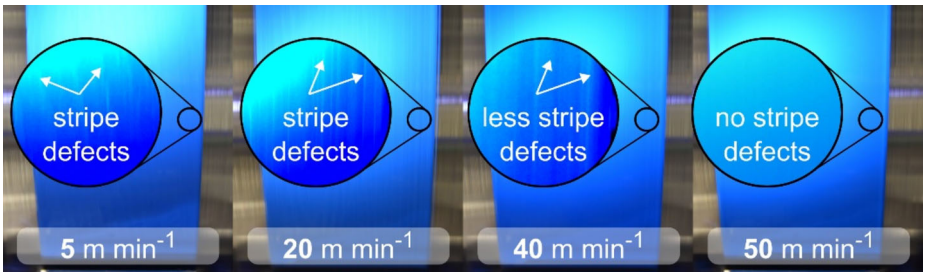

Fig. 9 Coating appearance at the slot die outlet for System-2 at a wet-film height of 200 µm at coating speeds from 5 to 50 m min^{-1}. Stripe defects are visible at low speeds and diminish with increasing speed until a stable coating is obtained at 50 m min.$^{-1}$

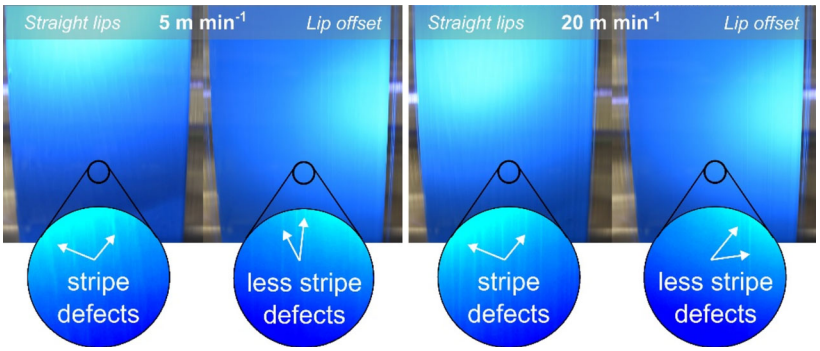

Fig. 10 Coating appearance at coating speeds of 5 and 20 m min^{-1} for straight-lip configuration vs. lip offset. The improvement in coating quality by introducing a lip offset is reflected in the reduction in the occurrence of stripe defects

5 and 20 m min^{-1} using the lip offset. Figure 10 illustrates the resulting comparison of the coating with a total wet-film thickness of 200 µm (bottom = 150 µm, top = 50 µm) with and without lip offset. For an improved visibility, the contrast in the excerpts shown for each coating was increased.

The analysis of the images indicates that the complete stabilization of the coating was not achieved. However, the quality has improved. The defect patterns have evolved from a multitude of broad, intersecting stripes to a few, exceedingly thin, linear stripes. Since the stripes have a light color, the defect can be assigned to an unstable lower layer. It is postulated that the viscosity ratio in the case of System-2 was excessive to be compensated for by a lip offset. Nevertheless, the introduction of a lip offset has proven to be a promising method for counteracting a combination of strong layer and viscosity ratios.

3.3 Electrode production (pilot line)

System-1 was used to produce electrodes at 1 m min^{-1} coating speed at the pilot plant. Regarding System-2, the production of electrodes was not possible due to the exceeding of the maximum coating speed of the pilot line by the requisite minimum coating speed for stable coatings.

Surface tension differences

The formulation study yielded several material combinations that exhibited not only distinct rheological properties but also distinctive surface tension characteristics. The surface tension varied by up to 15–20 mN m^{-1}. When the surface tension in the upper layer was greater than that in the lower layer with a sufficiently high difference, surface irregularities were observed that resembled the texture of an orange peel, building up after the die outlet. Figure 11 illustrates two multi-layer coatings, one exhibiting the orange peel effect (left) and the other a stable, smooth coating (right).

To systematically illustrate the impact, 2.5 wt% isopropanol was added to a portion of the battery slurry to reduce the surface tension, while another portion remained unaltered. These slurries were combined in two-layer coatings using a two-layer doctor blade. This leads to the formation of three distinct material combinations. In one, the surface tension of the upper layer is approximately equivalent to that of water (approximately 70 mN m^{-1}), while the lower layer exhibits a reduction in surface tension of approximately 12 mN m^{-1}. In the other, the configuration is reversed, with the lower layer exhibiting a higher surface tension. These configurations are subjected to a control experiment in which the same slurry with the high surface tension is used in both layers. Figure 12 presents images of the individual configurations.

It can be observed that the uneven surface is created by the unstable layer configuration with a higher surface tension in the lower layer. Conversely, if the configuration is reversed, no adverse effects on the surface quality

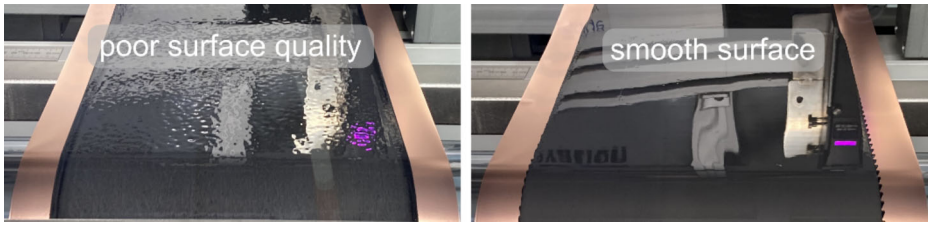

Fig. 11 Examples of two formulations with identical coating parameters, on the left a system with surface irregularities (orange skin effect) due to unstable layer configurations, on the right a system with a smooth surface

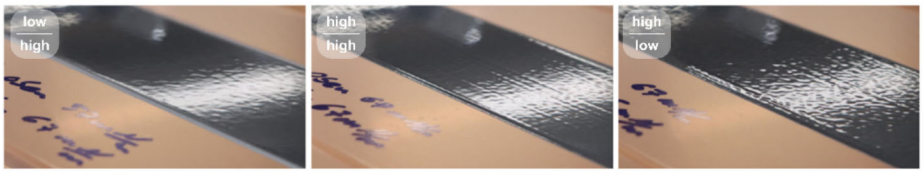

Fig. 12 Coatings of battery slurries with surface tension differences between the layers. High surface tension in the bottom layer (left), high surface tension in both layers (middle), and high surface tension in the top layer (right). Surface irregularities increase significantly if the top layer exhibits a higher surface tension

could be observed. It is, therefore, recommended that surface tension differences should be avoided, especially when the lower layer has a higher one.

Electrode characterization

System-1 was processed for two primer areal mass loading of 1.5 and 2 g m^{-2} (wet-film heights of 210 µm and 233 µm, respectively) and tested for adhesion strength. The areal mass loading of the anode electrode was kept constant at 65 g m^{-2} (wet-film height 140 µm). The adhesion strength for the single-layer anode electrodes and its subsequent variations are depicted in Fig. 13.

The results show an improvement in adhesion strength for two-layer configurations in comparison to the single-layer anode electrode. The adhesion strength of the electrode is significantly increased from 11.6 to 16.7 N m^{-1} using a primer with an area weight of 1.5 g m^{-2}, which corresponds to a percentage increase of 45%. In comparison, an additional increase in the areal mass loading has only a slight effect on the given system, with a further increase to 17.2 N m^{-1}, which corresponds to an increase of 48% in relation to the single layer. In general, it can be deduced that the simultaneous coating approach is beneficial for the mechanical electrode properties.

To ascertain the impact of the primer layers on battery performance, cells comprising pure single-layer anodes and multi-layer electrodes with primer are assembled and subjected to capacity retention testing. Initially, System-1, as illustrated in Fig. 14, is examined. To compare the capacity retention between single-layer anodes and anodes with primer layers, the measurements of two cells are presented.

The data of the single-layer anode electrodes show a high degree of similarity with a capacity retention of 92.3% after 400 cycles. The anodes with a primer layer exhibit a similar but slightly lower capacity retention of 91.8% and 91.4%. However, the difference between single- and multi-layer anode electrodes is not significant.

Combining the results of the adhesion strength and electrochemical tests, it is apparent that the simultaneous multi-layer approach is a promising option for material System-1. Further investigations should clarify whether it is possible to further reduce the binder content in the anode of the multi-layer while maintaining the adhesion strength, to achieve an improvement in the electrochemical performance as well.

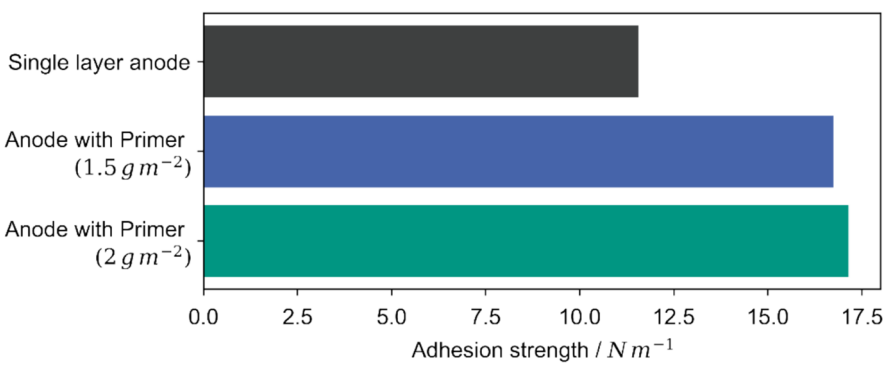

Fig. 13 Adhesion strength of calendered electrodes of System-1 with different primer area weights (0, 1.5 and 2 g m^{-2}). The utilization of the anode with primer demonstrated an increase in adhesion strength of 45% and 48%, respectively

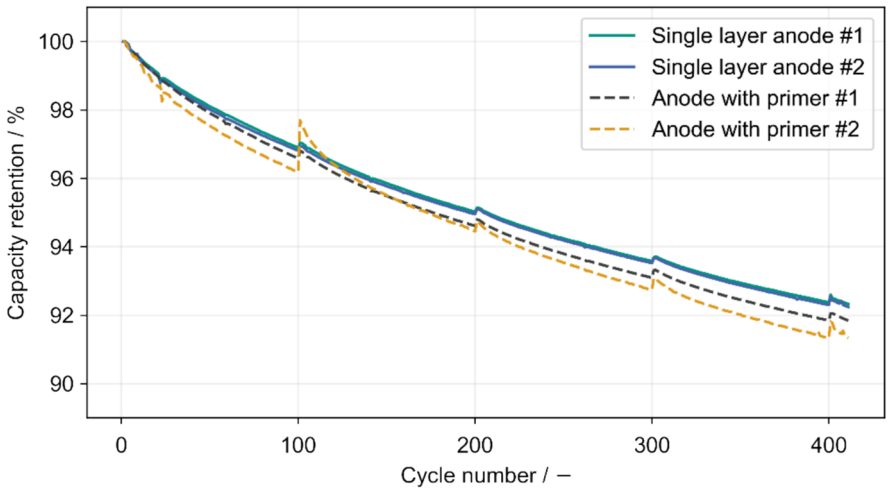

Fig. 14 Capacity retention of single-layer anodes and anodes with primer layer from System-1 over 400 cycles

4 Conclusion and outlook

Within this study, an investigation into the simultaneous two-layer coating of LIB anode electrodes with primer layers as a one-step approach was presented. The first part conducted an examination of coating stability. The viscosity profiles of the anode and primer slurries in material System-1 exhibited minor differences at low shear rates, which increased with higher shear rates. Conversely, in System-2, high-viscosity ratios at low shear rates were present, with viscosity profiles converging at higher shear rates. It was demonstrated that coating windows tend to be widest when viscosity profiles exhibit low disparities.

In System-1, the viscosity difference was generally small enough to produce stable coatings across the entire speed range from 5 to 50 m min^{-1}. However, in System-2, the viscosity ratio at low shear rates was too high to produce stable coatings at low coating speeds, so that stable regions were only found at coating speeds above 40 m min^{-1}, corresponding to the convergence of viscosity profiles at high shear rates. The study underscores the relevance of rheological properties and their ratios in multi-layer coatings, as they are crucial during scale-up or process speed alteration and may lead to an unstable process point necessitating further measures. To test such a measure, a lip offset was introduced to assess the potential for stabilizing process points at low speeds for System-2. A quality improvement was demonstrated; however, the viscosity ratio was too large to achieve fully homogeneous coating appearance.

Furthermore, a systematic combination of different surface tensions illustrated that those multi-layer coatings, where the upper layer exhibits higher surface tension than the lower layer, can produce strong irregularities in the coating surface.

From material System-1, electrodes were produced at the pilot line. Single-layered anode electrodes were fabricated as control experiments. The electrodes were calendered, tested for adhesion strength, and assembled into cells. In all cases, the adhesion strength significantly increased compared to the single-layer electrodes for primer area weights of 1.5 g m^{-2} (increase about 45%). Further increasing the area weight of the primer layer to 2 g m^{-2} had no considerable influence.

The electrochemical properties were evaluated in terms of capacity retention. The multi-layer electrodes showed a similar average capacity retention compared to the single-layer electrodes (92.3% vs 91.6%) after 400 cycles.

In conclusion, it can be stated that the simultaneous coating of multi-layer anode electrodes with primer layer results in enhanced mechanical electrode properties without significantly affecting the electrochemical performance. In contrast to the sequential coating process, only a single coating and drying step is required, which significantly reduces the investment cost for plant components. The results of this study show that the use of primers creates new opportunities for optimizing electrodes. In the future, it is advisable to investigate the possibility to further reduce the binder content in the anode, to achieve not only an improvement in the mechanical quality but also in the electrochemical performance. Moreover, an investigation into the potential acceleration and optimization of the drying process, when compared to the sequential approach, is recommended. This inquiry should be complemented by a methodical investigation on the stability of multi-layer coatings for non-Newtonian fluids. Emphasis should be placed on discerning the impact of viscosity ratios and wet-film height ratios, alongside the influence of coating speed, creating the link between rheological behavior and coating stability. In addition, the parameters that determine the onset of intermixing require further investigation, along with strategies for manipulating coating

beads, which include considerations such as the introduction of a lip offset, usage of an angle of attack or a vacuum box.

Supplementary Information The online version contains supplementary material available at https://doi.org/10.1140/epjs/s11734-024-01398-7.

Acknowledgements The authors would like to acknowledge financial support of the Federal Ministry of Education and Research (BMBF) via the research project ForeCast (Grant No.: 03XP0402B).

Funding Open Access funding enabled and organized by Projekt DEAL. The funding has been received from Bundesministerium für Bildung und Forschung with Grant no. 03XP0402B.

Data availability The authors declare that the raw data used in this study are available in the Supplementary Information files.

References

1. L. Mauler, F. Duffner, W.G. Zeier, J. Leker, Battery cost forecasting: a review of methods and results with an outlook to 2050. Energy Environ Sci **14**, 4712–4739 (2021). https://doi.org/10.1039/D1EE01530C
2. S. Jaiser, M. Müller, M. Baunach, S. Scharfer et al., Investigation of film solidification and binder migration during drying of Li-Ion battery anodes. J. Power Sour. **318**, 210–219 (2016). https://doi.org/10.1016/j.jpowsour.2016.04.018
3. S. Jaiser, L. Funk, M. Baunach, S. Scharfer et al., Experimental investigation into battery electrode surfaces: the distribution of liquid at the surface and the emptying of pores during drying. J. Colloid Interface Sci. **494**, 22–31 (2017). https://doi.org/10.1016/j.jcis.2017.01.063
4. M. Müller, L. Pfaffmann, S. Jaiser et al., Investigation of binder distribution in graphite anodes for lithium-ion batteries. J. Power Sour. **340**, 1–5 (2017). https://doi.org/10.1016/j.jpowsour.2016.11.051
5. J. Klemens, D. Burger, L. Schneider, S. Scharfer et al., Drying of compact and porous NCM cathode electrodes in different multilayer architecture—influence of layer configuration and drying rate on electrode properties. Energy Technol. (2023). https://doi.org/10.1002/ente.202300267
6. R. Morasch, J. Landesfeind, B. Suthar, H.A. Gasteiger, Detection of binder gradients using impedance spectroscopy and their influence on the tortuosity of li-ion battery graphite electrodes. J. Electrochem. Soc. **165**, A3459 (2018). https://doi.org/10.1149/2.1021814jes
7. J. Klemens, L. Schneider, D. Burger, S. Scharfer et al., Process and drying behavior toward higher drying rates of hard carbon anodes for sodium-ion batteries with different particle sizes: an experimental study in comparison to graphite for lithium-ion-batteries. Energy Tech **11**, 2300338 (2023). https://doi.org/10.1002/ente.202300338
8. J. Kumberg, W. Bauer, J. Schmatz, S. Scharfer et al., Reduced drying time of anodes for lithium-ion batteries through simultaneous multilayer coating. Energy Technol **9**, 2100367 (2021). https://doi.org/10.1002/ente.202100367
9. R. Diehm, J. Kumberg, C. Dörrer, S. Scharfer et al., In situ investigations of simultaneous two-layer slot die coating of component-graded anodes for improved high-energy li-ion batteries. Energy Technol **8**, 1901251 (2020). https://doi.org/10.1002/ente.201901251
10. R. Diehm, M. Müller, D. Burger, S. Scharfer et al., High-speed coating of primer layer for li-ion battery electrodes by using slot-die coating. Energy Technol **8**, 2000259 (2020). https://doi.org/10.1002/ente.202000259
11. P.M. Schweizer, *Premetered coating methods* (Springer International Publishing, Cham, 2022)
12. H.S. Ji, W.-G. Ahn, I. Kwon et al., Operability coating window of dual-layer slot coating process using viscocapillary model. Chem. Eng. Sci. **143**, 122–129 (2016). https://doi.org/10.1016/j.ces.2015.12.016
13. J. Nam, M.S. Carvalho, Mid-gap invasion in two-layer slot coating. J. Fluid Mech. **631**, 397–417 (2009). https://doi.org/10.1017/S0022112009007022
14. J. Nam, M.S. Carvalho, Two-layer tensioned-web-over-slot die coating: effect of die lip geometry. Chem. Eng. Sci. **65**, 4014–4026 (2010). https://doi.org/10.1016/j.ces.2010.03.044
15. J.S. Park, T. Yoo, B. Chun et al., Operability limits for non-newtonian liquids in dual-layer slot coating processes using the viscocapillary model. J. Coat. Technol. Res. **19**, 35–47 (2022). https://doi.org/10.1007/s11998-021-00499-5
16. M. Schmitt, S. Raupp, D. Wagner, S. Scharfer et al., Analytical determination of process windows for bilayer slot die coating. J. Coat. Technol. Res. **12**, 877–887 (2015). https://doi.org/10.1007/s11998-015-9701-4